Research Article Vol. 34, No. 6 / June 2017 / Journal of the Optical Society of America B 1255

Journal of the Optical Society of America B

OPTICAL PHYSICS

Measurement of dispersive profile of a multiwindow electromagnetically induced transparency spectrum in a Doppler-broadened atomic medium

Dinh Xuan Khoa, Le Canh Trung, Phan Van Thuan, Le Van Doai, and Nguyen Huy Bang*

Vinh University, 182 Le Duan Street, Vinh City, Vietnam
**Corresponding author: bangnh@vinhuni.edu.vn*

Received 14 February 2017; revised 27 April 2017; accepted 29 April 2017; posted 3 May 2017 (Doc. ID 286690); published 26 May 2017

We have measured the dispersive profile of a multiwindow electromagnetically induced transparency (EIT) spectrum in a medium consisting of Rb atoms in the presence of Doppler broadening. The atomic medium is excited by a strong coupling light and a weak probe laser light via the V-type transitions within the D_2 manifold. Under the EIT effect, an anomalous dispersive region of the medium is basically modified into multinormal and anomalous dispersive regions. Furthermore, the slope and position of the dispersion can be controlled with the intensity and frequency of the coupling light. An analytic model is proposed to simulate the observed spectrum with a good agreement. Such controllable dispersive properties with their analytic description would be useful for finding applications related to multiwindow EIT phenomena. © 2017 Optical Society of America

OCIS codes: (020.1670) Coherent optical effects; (160.2710) Inhomogeneous optical media; (160.4760) Optical properties.

https://doi.org/10.1364/JOSAB.34.001255

1. INTRODUCTION

Electromagnetically induced transparency (EIT) is a quantum interference effect that leads to reduction of resonant absorption for a weak probe laser beam propagating through an opaque medium induced by a strong coupling laser field. The theory of EIT was first proposed in 1989 [1] and experimentally verified in 1991 [2]. Since then, EIT has attracted tremendous interest [3–7] due to its unusual optical properties and promising potential applications, for example, lasing without inversion [8], high resolution spectroscopy [9], nonlinear optics at low light intensities [10], and so on.

In addition to reduction of the resonant absorption, a basic modification of the dispersive property of the EIT medium is also interesting for both theoretical [11,12] and experimental [6,13] studies. It is shown that very steep slopes of dispersion of the EIT medium can slow down the group velocity of light [14,15], and even stop and store the light pulse in an atomic medium [16,17]. These effects deliver several applications, such as giant Kerr nonlinearity [18–20], optical bistability [21,22], all-optical switching [23,24], quantum memory devices, and generation of photonic qubits [25,26].

The early studies of EIT were mainly focused on three-level configurations, including cold [5,7] and hot [3,4] gaseous media that give rise to a single-window EIT. Recently, extension from single- to multiwindow EIT has also been performed diversely [12,27–32]. In this issue, one can simultaneously slowlight pulses at different frequencies [30,31], which has some advantages in the production of quantum entanglement [32]. Other studies of multiwindow EIT relate to velocity selection [33,34], optical nanofiber for guided entangled beams [35], and the influence of external magnetic field [36].

A promising way to create multiwindow EIT is use of closely spaced hyperfine levels in atomic systems where a strong light field can simultaneously couple the levels. This was first realized by Wang *et al.* [37] for a five-level cascade type of cold ^{85}Rb atoms in a magneto-optical trap. The observation was recently simulated by an analytic model [38], which is useful for finding related applications, such as generation of guided entangled beams and all-optical switching in optical nanofibers [35]. Growing interest in EIT is also extended to hot gaseous media due to its close-to-normal condition and because it has some interesting effects, such as narrowing the EIT linewidth [39].

From the practical point of view, the number of measurements on absorption EIT spectrum is huge but that of dispersion is still very modest [6,13], particularly for multiwindow EIT. This contrasts with the fact that most applications of the EIT concern dispersive properties. As in several related applications, an accurate control of the dispersive property of the multiwindow EIT medium under Doppler broadening is desired to optimize the related processes, for example,

simultaneous control of group velocity of light pulses in a quantum information system [40], high-sensitivity optical magnetometers [41], and dispersion management in optical communication systems. In order to partially meet these needs, in this work, we measure the dispersive profile of multiwindow EIT in a ^{85}Rb atomic medium under Doppler broadening. A simple analytic model is developed to fit with observed data for delivering related applications.

2. EXPERIMENTAL ARRANGEMENT AND THEORETICAL MODEL

In this experiment, the ^{85}Rb atomic gaseous sample is produced in a Rb cell with a temperature controller. Two single-mode extended-cavity diode lasers DL1 and DL2 (with 4 mm beam diameter, ≈1 MHz linewidth, and operating around 780 nm) are used to excite transitions on the D_2 manifold of the ^{85}Rb atomic system, as shown in Fig. 1. The strong coupling beam with a fixed frequency ω_c (and Rabi frequency Ω_c) simultaneously couple the hyperfine ground state $5S_{1/2}$ ($F = 3$) with the three excited states $5P_{3/2}$ ($F' = 2, 3, 4$), whereas the weak probe beam with frequency ω_p (and Rabi frequency Ω_p) scans over the same transitions from the $5S_{1/2}$ ($F = 3$) state to $5P_{3/2}$ ($F' = 2$, 3, 4) states. We denote δ_1 and δ_2 as frequency separations between the $|2\rangle - |3\rangle$ levels and $|3\rangle - |4\rangle$ levels, respectively.

The experimental arrangement for measuring absorption and dispersion spectra is similar to that described in [42], except an additional part here is use of the coupling laser DL2 to induce EIT effect in the sample, as shown in Fig. 2. In a brief description of the setup, the output light of the laser DL1 is split by the beam splitter BS1 into a small part and then is directed to a Fabry–Perot interferometer (FPI; with a free-spectral range, FRS = 378 MHz) for calibration of the observed spectrum, whereas the remaining one is directed to a second beam splitter (BS2), which is the entrance of a Mach–Zehnder interferometer (MZI). The MZI consists of two 50% beam splitters (BS2 and BS3) and two dielectric mirrors (M_1 and M_2). Each mirror or beam splitter of the MZI is mounted on a three-axis microtranslation stage to perform precise control of optical paths. The length of each arm of the MZI is about 20 cm, and both arms are arranged so that the difference of their lengths is much smaller than 1.5 cm [42]. The Rb cell with two quarter-waveplates, QW1 and QW2 (at both ends of the cell), are placed in the second arm of the MZI. The output beam of the DL2 laser is split in two parts; the first one is directed to the Rb cell as the coupling

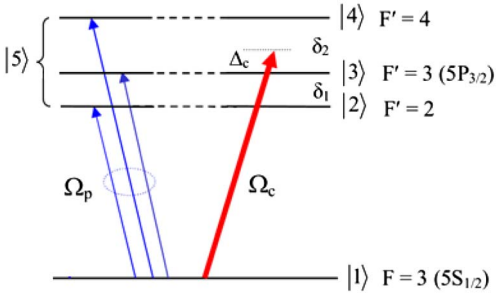

Fig. 1. Excitation scheme of a multilevel V-type system in ^{85}Rb atoms.

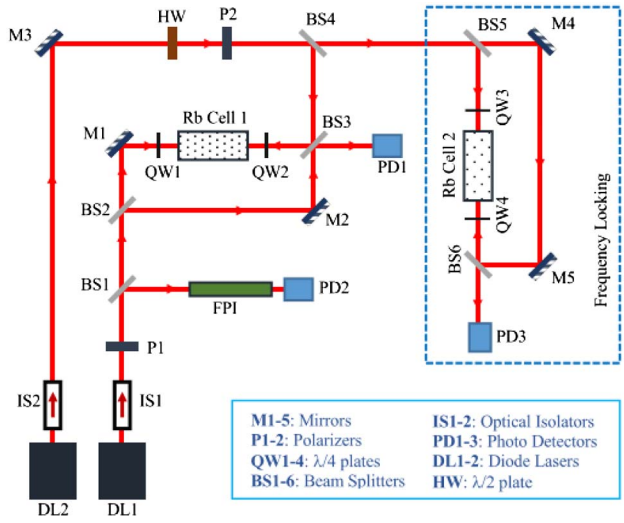

Fig. 2. Optical layout of the experimental arrangement: two diode lasers DL1 and DL2 are used to deliver probe and coupling lights, respectively. The dashed border indicates a saturation spectroscopy setup for locking frequency of the coupling laser DL2.

light to induce the EIT effect, and the second part is directed to a saturated absorption spectroscopic setup (within the dashed border in Fig. 2) to lock the frequency of the coupling laser to a hyperfine transition.

Whenever absorption spectrum is being measured, the first arm of the MZI is blocked to avoid influence of interference on the recorded absorption spectrum. We used a combination of half-wave plates and polarizers to control the intensity of the coupling and probe lights. In our measurements, the power of the probe light is reduced to a few microwatts, whereas the intensity of the coupling light is changed from a few tens of milliwatts. The probe and FPI signals are recorded simultaneously by two photodiodes, PD1 and PD2, respectively.

In order to describe the experimental observations, we use the density matrix formalism. In the electric dipole approximation, the evolution of system is governed by the Liouville equation:

$$\dot{\rho} = -\frac{i}{\hbar}[H, \rho] + \Lambda\rho, \tag{1}$$

where $\Lambda\rho$ represents the decay mechanisms inside the atomic system. In our experiments, the probe light is scanned over transitions from the $5S_{1/2}$ ($F = 3$) state to $5P_{3/2}$ ($F' = 2$, 3, 4) states, and the absorption (α) and dispersion (n) coefficients are determined by

$$\alpha \propto \sum_{j=2}^{4} \mathrm{Im}(\rho_{j1}), \tag{2a}$$

$$n \propto \sum_{j=2}^{4} \mathrm{Re}(\rho_{j1}). \tag{2b}$$

Because the probe laser scans over transitions from the $5S_{1/2}$ ($F = 3$) state to $5P_{3/2}$ ($F' = 2$, 3, 4) states, the sums in Eqs. (2a) and (2b) are relatively lengthy for an analytical calculation. Indeed, such transitions can be decomposed into three combinations of four-level V-type excitation schemes, each of

which gives rise to two EIT windows. However, the position of each EIT window is determined by two photon-resonant conditions that lead to three of them being coincident; that is, only three EIT windows are observed separately. As indicated in [28], such a three-window EIT can therefore be modeled by a five-level excitation system in which a "virtue" level $|5\rangle$ represents either level $|2\rangle$, $|3\rangle$, or $|4\rangle$ for the probe transitions in a manner so that the coupling and probe transitions are not identical (see Fig. 1). For such an equivalent model, the coupling beam still simultaneously drives transitions between the state $|1\rangle$ and the states $|2\rangle$, $|3\rangle$, and $|4\rangle$, whereas the probe beam only excites a transition $|1\rangle \leftrightarrow |5\rangle$. The replacement of the three levels in the probe transitions is mathematically equivalent to what was done in [43]; thus the probe response is determined via the coherence of the term ρ_{51} as follows:

$$\rho_{51} \equiv \sum_{j=2}^{4} \mathrm{Re}(\rho_{j1}). \tag{3}$$

From Eq. (1), using the rotating-wave approximation, the coherent matrix elements of the five-level system are derived as

$$\dot{\rho}_{51} = [i\Delta_p - \gamma_{51}]\rho_{51} - \frac{i}{2}\Omega_p(\rho_{55} - \rho_{11}) + \frac{i}{2}\Omega_c a_{21}\rho_{52} + \frac{i}{2}\Omega_c a_{31}\rho_{53} + \frac{i}{2}\Omega_c a_{41}\rho_{54}, \tag{4}$$

$$\dot{\rho}_{52} = [i(\Delta_p - \Delta_c + \delta_1) - \gamma_{21}]\rho_{52} - \frac{i}{2}\Omega_p\rho_{12} + \frac{i}{2}\Omega_c a_{21}\rho_{51}, \tag{5}$$

$$\dot{\rho}_{53} = [i(\Delta_p - \Delta_c) - \gamma_{31}]\rho_{53} - \frac{i}{2}\Omega_p\rho_{13} + \frac{i}{2}\Omega_c a_{31}\rho_{51}, \tag{6}$$

$$\dot{\rho}_{54} = [i(\Delta_p - \Delta_c + \delta_2) - \gamma_{41}]\rho_{54} - \frac{i}{2}\Omega_p\rho_{14} + \frac{i}{2}\Omega_c a_{41}\rho_{51}, \tag{7}$$

where

$$\Omega_p = d_{51}E_p/\hbar, \qquad \Omega_c = d_{31}E_c/\hbar, \tag{8}$$

are Rabi frequencies for the probe and coupling light fields, respectively;

$$\Delta_p = \omega_p - \omega_{51}, \qquad \Delta_c = \omega_c - \omega_{31}, \tag{9}$$

are the frequency detuning of the coupling and probe beams, respectively;

$$a_{21} = d_{21}/d_{31}, \qquad a_{31} = d_{31}/d_{31}, \qquad a_{41} = d_{41}/d_{31}, \tag{10}$$

are the relative transition strengths of the three transitions from the three hyperfine sublevels $|2\rangle$, $|3\rangle$, and $|4\rangle$ to level $|3\rangle$; d_{ik} is the transition dipole moment between the states $|i\rangle$ and $|k\rangle$; and γ_{ik} represents the decay rates of the atomic coherence ρ_{ik}, given by [38]

$$\gamma_{ik} = \frac{1}{2}\left(\sum_{E_j<E_i}\Gamma_{ij} + \sum_{E_l<E_k}\Gamma_{kl}\right), \tag{11}$$

where Γ_{ik} is the decay rate of the population from level $|i\rangle$ to level $|k\rangle$. The laser linewidths, $\delta\omega_p$ and $\delta\omega_c$, are taken into account by including them in the decay rates, $\gamma_{21} \to \gamma_{21} + \delta\omega_c$, $\gamma_{31} \to \gamma_{31} + \delta\omega_c$, $\gamma_{41} \to \gamma_{41} + \delta\omega_c$ and $\gamma_{51} \to \gamma_{51} + \delta\omega_p$. For our experiments, we estimate $\delta\omega_p = \delta\omega_c = 1$ MHz.

In a weak field limit of the probe light intensity, the matrix element ρ_{51} can be determined at the steady regime as

$$\rho_{51} = \frac{\frac{i}{2}\Omega_p}{F}, \tag{12}$$

where

$$F = \gamma_{51} - i\Delta_p + \frac{a_{31}^2(\Omega_c/2)^2}{\gamma_{31} - i(\Delta_p - \Delta_c)} + \frac{a_{21}^2(\Omega_c/2)^2}{\gamma_{21} - i(\Delta_p - \Delta_c + \delta_1)} + \frac{a_{41}^2(\Omega_c/2)^2}{\gamma_{41} - i(\Delta_p - \Delta_c - \delta_2)}. \tag{13}$$

The linear susceptibility of the atomic medium for the probe light field relates to the matrix element ρ_{51} as follows:

$$\chi = 2\frac{Nd_{51}}{\epsilon_0 E_p}\rho_{51}. \tag{14}$$

In the presence of the Doppler effect, additional shifts of frequency detuning of the coupling and probe light fields should be taken into account. Because the probe and coupling beams counterpropagate in the medium, a moving atom with velocity v toward the probe beam will therefore "see" a frequency upshift (by $+\omega_p v/c$) and downshift (by $-\omega_p v/c$) for the probe and coupling lights, respectively. Under such Doppler shifts, the frequency detunings are modified to

$$\Delta_p = \omega_p - \omega_{51} + \omega_p v/c; \qquad \Delta_c = \omega_c - \omega_{31} - \omega_c v/c. \tag{15}$$

In a thermal equilibrium condition at temperature T, the number of atoms having velocity v is represented by the Maxwell–Boltzmann distribution,

$$N(v) = \frac{N_0}{u\sqrt{\pi}}e^{-v^2/u^2}dv, \tag{16}$$

where

$$u = \sqrt{\frac{2k_B T}{m}} \tag{17}$$

is the most probable velocity and m is the mass of the particle; N_0 is the total number of particles occupied in a volume unit.

Under these assumptions of the Doppler effect, the linear susceptibility in Eq. (13) is integrated over the velocity v as

$$\chi = \int_{-\infty}^{+\infty}\chi(v)\mathrm{d}v = \frac{iN_0 d_{51}^2\sqrt{\pi}}{\epsilon_0\hbar(\omega_p u/c)}e^{z^2}[1 - \mathrm{erf}(z)], \tag{18}$$

where $\mathrm{erf}(z)$ is the error function of a complex argument z:

$$z = \frac{c}{\omega_p u} \times F. \tag{19}$$

According to the Kramers–Kronig relation, the imaginary (χ'') and real (χ') parts of the linear susceptibility correspond to the absorption and dispersion coefficients, respectively, $\chi = \chi' + \chi''$. The absorption and dispersion coefficients for the probe light are therefore given by

$$\alpha = \frac{\omega_p n_0 \chi''}{c}, \tag{20}$$

$$n = \frac{\omega_p n_0 \chi'}{2c}, \tag{21}$$

where n_0 is the background index of refraction [13].

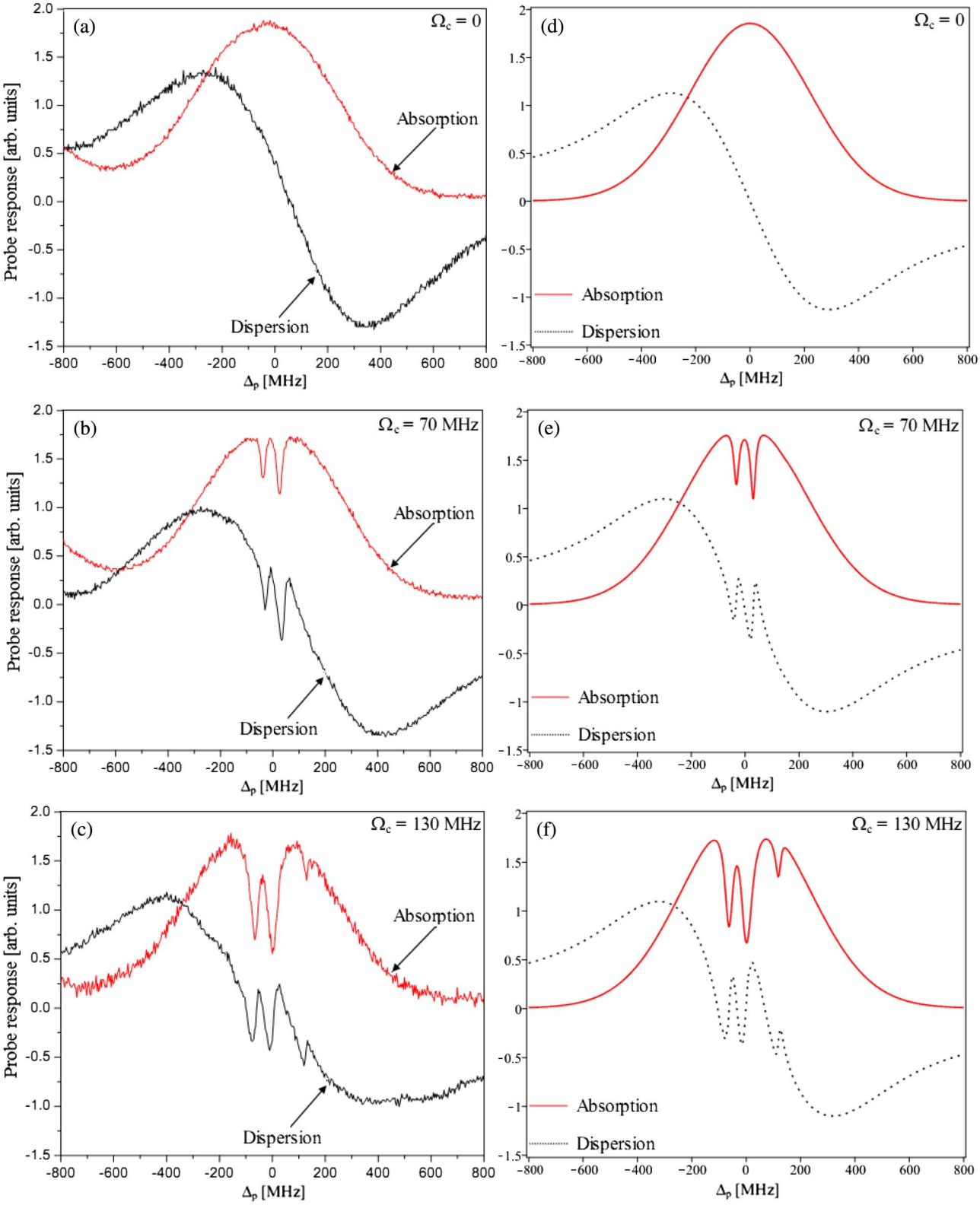

Fig. 3. Experimental observations (a,b,c) and theoretical simulations (d,e,f) of the absorption (solid curve) and dispersion (dotted curve) spectra of the probe light for various coupling intensities Ω_c (indicated in figures) when frequency detuning $\Delta_c = 0$ and $T = 300$ K.

For a quantitative description, we often use the so-called transparent efficiency (R_{EIT}), which is defined by the following relation:

$$R_{EIT} = \frac{\alpha_{off} - \alpha_{on}}{\alpha_{off}} \times 100\%, \quad (22)$$

where α_{on} and α_{off} denote the absorption coefficient for the cases where the coupling light beam is on and off, respectively.

In addition to R_{EIT}, fullwidths at half-maxima (FWHMs) of the EIT windows which correspond to the coupling transitions $|1\rangle \leftrightarrow |2\rangle$, $|1\rangle \leftrightarrow |3\rangle$, and $|1\rangle \leftrightarrow |4\rangle$ are given by [39]

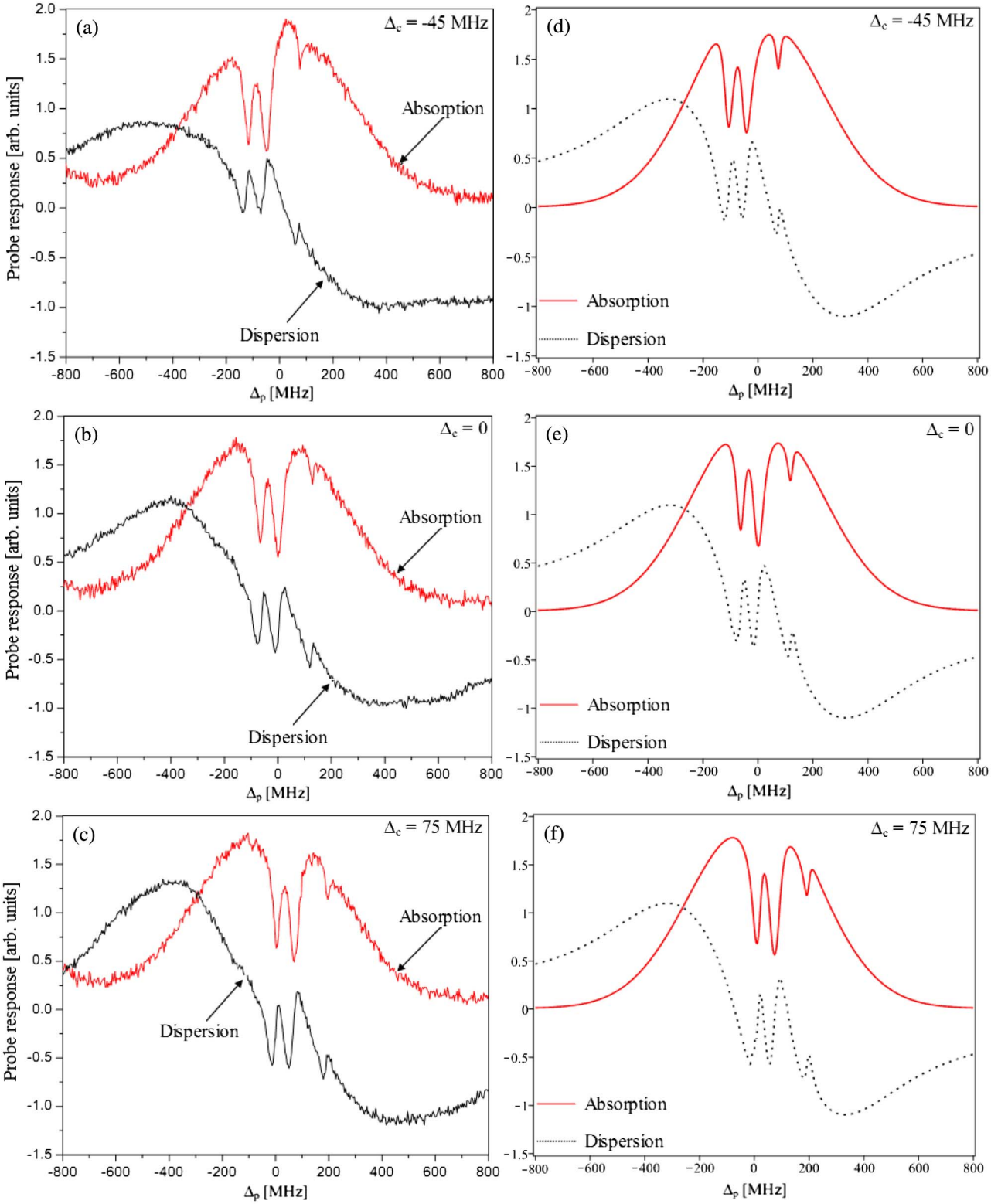

Fig. 4. Experimental observation (a,b,c) and theoretical calculation (d,e,f) of absorption and dispersion spectra (at $\Omega_c = 130$ MHz and $T = 300$ K) for different values of Δ_c.

$$\mathrm{FWHM}_{21} = \frac{a_{21}^2 \Omega_c^2}{4(W_D + \gamma_{21})}, \tag{23}$$

$$\mathrm{FWHM}_{31} = \frac{a_{31}^2 \Omega_c^2}{4(W_D + \gamma_{31})}, \tag{24}$$

$$\mathrm{FWHM}_{41} = \frac{a_{41}^2 \Omega_c^2}{4(W_D + \gamma_{41})}, \tag{25}$$

where W_D is the Doppler width, given by

$$W_D = \frac{2\omega_p}{c} u\sqrt{\ln 2} = \frac{\omega_p}{c}\sqrt{\frac{8k_B T \ln 2}{m}}. \tag{26}$$

3. EXPERIMENTAL RESULTS AND THEORETICAL SIMULATIONS

In a first step, the coupling laser frequency is tuned resonantly to the transition $5S_{1/2}(F = 3) \leftrightarrow 5P_{3/2}(F' = 3)$ while the probe laser is scanned over the transitions $5S_{1/2}(F = 3) \leftrightarrow 5P_{3/2}(F' = 2, 3, 4)$. The temperature of a rubidium vapor cell is stabilized at $T = 300$ K. The absorption and dispersion profiles for various coupling intensities are shown as in Fig. 3, where the left and right columns represent the experimental and theoretical spectra, respectively. In our theoretical simulations, the atomic parameters are chosen as follows [44]: $\delta_1 = 63.4$ MHz, $\delta_2 = 120.6$ MHz, $\gamma_{21} = \gamma_{31} = \gamma_{41} = \gamma_{51} = 7.5$ MHz. We fit the experimental data with Eqs. (20) and (21) for various ratios of relative coupling strengths; the finally optimized results are $a_{21} : a_{31} : a_{41} = 0.8 : 1 : 0.3$.

Figures 3(a) and 3(d) show the probe absorption and dispersion spectra without the coupling light ($\Omega_c = 0$). In this case, we see a Lorentzian absorption and its dispersion profile. When the coupling power is increased to 3.5 mW, which corresponds to a value of Rabi frequency $\Omega_c = 70$ MHz [Figs. 3(b) and 3(e)], the absorption spectrum appears as apparently two EIT windows whereas the dispersion is modified in the region of each EIT window. This modification of absorption and dispersion is consistent with the Kramers–Kronig relation. By increasing the coupling power up to 12 mW, which corresponds to $\Omega_c = 130$ MHz, a third EIT window occurs [the window on the right of Figs. 3(c) and 3(f)]. The third window occurred only at higher power of the coupling light because the relative transition strength a_{41} corresponding to this window is quite small. The frequency separations between the three EIT windows are 63.4 and 120.6 MHz, the same as the separations δ_1 and δ_2, respectively. By comparing Fig. 3(a) with Fig. 3(c) one can see a basic modification of dispersion under the EIT effect. Furthermore, within each EIT window there is an anomalous–normal region of dispersion, which is consistent with the Kramers–Kronig relation.

In the next step, the absorption and its dispersion spectrum are measured at negative, zero, and positive values of the detuning Δ_c with a fixed coupling power at 12 mW (corresponding to $\Omega_c = 130$ MHz) as shown in the left column (Fig. 4). From the observations, we see a systematic shift of EIT windows and their dispersion profiles to the red or blue side when the coupling laser frequency shifts to red or blue directions, respectively. As explained in [45], the physics reason for these shifts is that the positions of the EIT windows are determined by the two-photon resonant condition, namely, $\Delta_p = \Delta_c$.

In order to quantitatively study the influence of the coupling light intensity on the EIT spectrum, we measured the EIT efficiency (R_{EIT}) and EIT width (FWHM) of each EIT window for several values of Rabi frequency Ω_c, as shown by squares in Figs. 5 and 6, respectively. In these figures, the solid lines represent the calculation from Eqs. (22)–(26) in accordance with the experimental parameters. Here, one can see different slopes of the curves, which are attributed to the different values of the effective coupling strengths; see Eq. (10). As a result, for a given coupling power, there is a broader EIT width corresponding the transition $|1\rangle \leftrightarrow |3\rangle$ and a narrower width for the transition $|1\rangle \leftrightarrow |4\rangle$ (see Fig. 6). On the other hand, the width of each EIT window is increased with increasing power of the coupling light [see Eqs. (23)–(25)]. This also leads to shadowing the slopes of the normal and anomalous dispersive curves (power broadening becomes significant).

Finally, the coupling laser is tuned to resonance with the transition $|1\rangle \leftrightarrow |3\rangle$ while its power is fixed at 42 mW (corresponding to $\Omega_c = 240$ MHz), and measured absorption for various values of temperature, as indicated in Fig. 7. It is shown that growing of temperature leads to lower EIT depth and

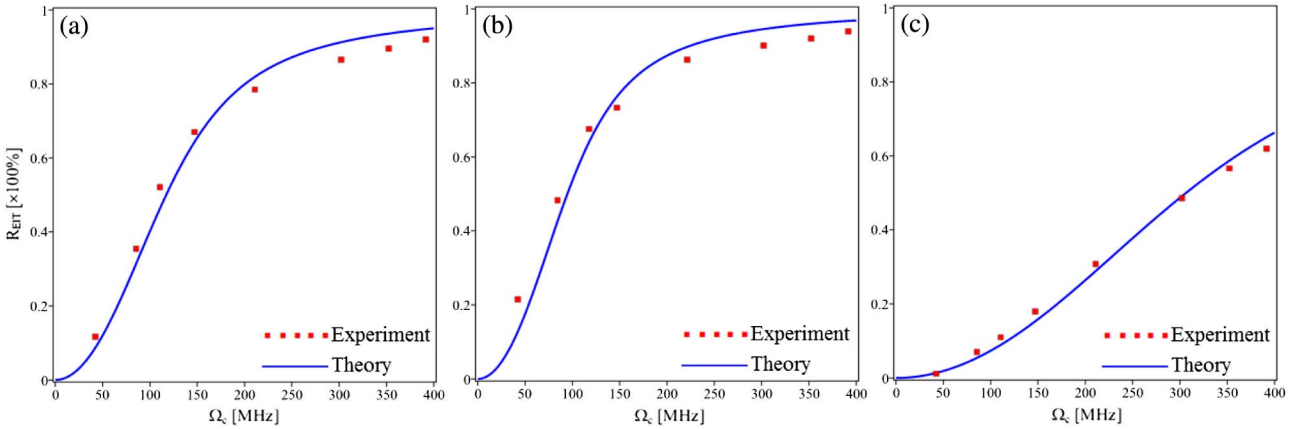

Fig. 5. Influence of Rabi frequency Ω_c on R_{EIT} induced by the coupling transitions (a) $|1\rangle \leftrightarrow |2\rangle$, (b) $|1\rangle \leftrightarrow |3\rangle$, and (c) $|1\rangle \leftrightarrow |4\rangle$ when $T = 300$ K. The squares and solid lines represent experiment and theory, respectively.

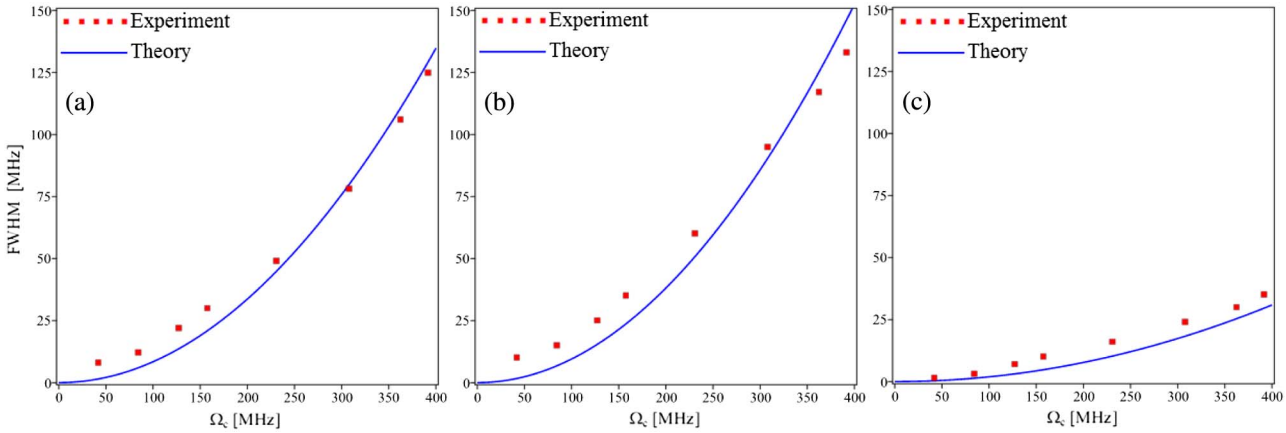

Fig. 6. Influence of Rabi frequency Ω_c on FWHM induced by the coupling transitions (a) $|1\rangle \leftrightarrow |2\rangle$, (b) $|1\rangle \leftrightarrow |3\rangle$, and (c) $|1\rangle \leftrightarrow |4\rangle$ when $T = 300$ K. The squares and solid lines represent experiment and theory, respectively.

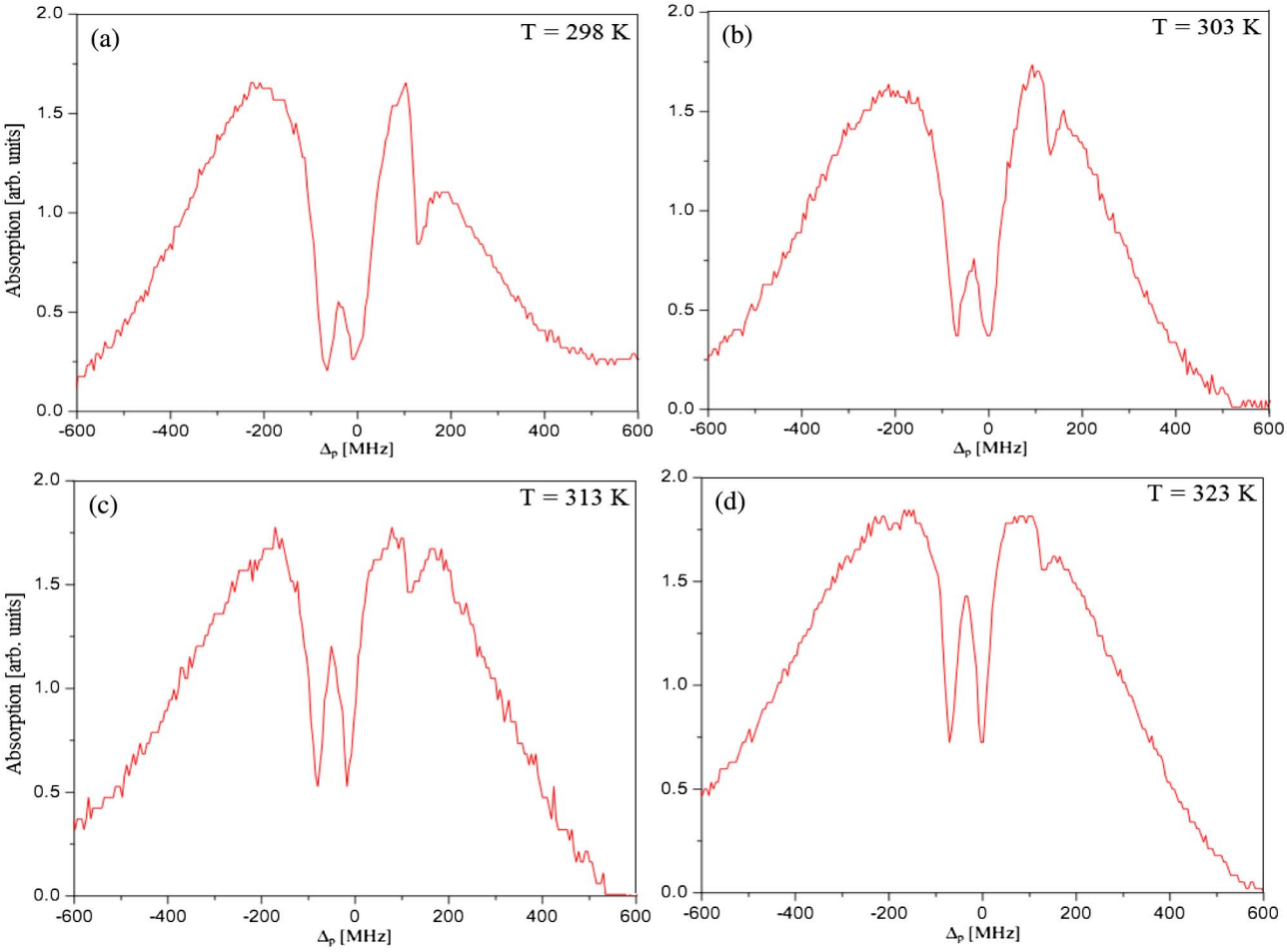

Fig. 7. Absorption spectrum of atomic medium measured at $\Omega_c = 240$ MHz and $\Delta_c = 0$ for various temperatures, (a) 298 K, (b) 303 K, (c) 313 K, and (d) 323 K.

narrower EIT width. The physical reasons to explain this tendency are attributed to reduction of atomic coherence as thermal atomic motion grows, and growth of atomic density [45] as the Rb cell is heated over the melting point of Rb (about 312 K [44]).

4. CONCLUSION

We have studied dispersion of a multiwindow EIT in a ^{85}Rb atomic gaseous medium under Doppler broadening. The dispersive profile of a three-window EIT spectrum has been

measured for various values of the parameters of the coupling light and temperature of the Rb cell. We observed multinormal and anomalous dispersion, which is controllable by a coupling light (intensity and/or frequency) or changing the temperature of the medium. An analytic model including the Doppler effect is also developed to describe the experimental observations with a good agreement. The obtained experimental results and the proposed analytic model can be useful for various applications related to multiwindow EIT phenomena.

Funding. Vietnam's Ministry of Science and Technology (ĐTĐLCN.17/17).

REFERENCES

1. A. Imamoğlu and S. E. Harris, "Lasers without inversion: interference of dressed lifetime-broadened states," Opt. Lett. **14**, 1344–1346 (1989).
2. K. J. Boller, A. Imamoglu, and S. E. Harris, "Observation of electromagnetically induced transparency," Phys. Rev. Lett. **66**, 2593–2596 (1991).
3. Y.-Q. Li and M. Xiao, "Electromagnetically induced transparency in a three-level Λ-type system in rubidium atoms," Phys. Rev. A **51**, R2703–R2706 (1995).
4. Y.-Q. Li and M. Xiao, "Electromagnetically induced transparency in ladder-type inhomogeneously broadened media: theory and experiment," Phys. Rev. A **51**, 576–584 (1995).
5. S. A. Hopkins, E. Usadi, H. X. Chen, and A. V. Durrant, "Electromagnetically induced transparency of laser-cooled rubidium atoms in three-level Λ-type systems," Opt. Commun. **138**, 185–192 (1997).
6. J. Zhao, L. Wang, L. Xiao, Y. Zhao, W. Yin, and S. Jia, "Experimental measurement of absorption and dispersion in V-type cesium atom," Opt. Commun. **206**, 341–345 (2002).
7. V. Ahufinger, R. Corbalan, F. Cataliotti, S. Burger, F. Minardi, and C. Fort, "Electromagnetically induced transparency in a Bose–Einstein condensate," Opt. Commun. **211**, 159–165 (2002).
8. A. S. Zibrov, M. D. Lukin, D. E. Nikonov, L. Hollberg, M. O. Scully, V. L. Velichansky, and H. G. Robinson, "Experimental observation of laser oscillation without population inversion via quantum interference in Rb," Phys. Rev. Lett. **75**, 1499–1502 (1995).
9. A. Krishna, K. Pandey, A. Wasan, and V. Natarajan, "High-resolution hyperfine spectroscopy of excited states using electromagnetically induced transparency," Europhys. Lett. **72**, 221–227 (2005).
10. S. E. Harris and L. V. Hau, "Nonlinear optics at low light levels," Phys. Rev. Lett. **82**, 4611–4614 (1999).
11. S. E. Harris, J. E. Field, and A. Kasapi, "Dispersive properties of electromagnetically induced transparency," Phys. Rev. A **46**, R29–R32 (1992).
12. A. Joshi and M. Xiao, "Electromagnetically induced transparency and its dispersion properties in a four-level inverted-Y atomic system," Phys. Lett. A **317**, 370–377 (2003).
13. M. Xiao, Y.-Q. Li, S.-Z. Jin, and J. Gea-Banacloche, "Measurement of dispersive properties of electromagnetically induced transparency in rubidium atoms," Phys. Rev. Lett. **74**, 666–669 (1995).
14. L. V. Hau, S. E. Harris, Z. Dutton, and C. H. Bejroozi, "Light speed reduction to 17 metres per second in an ultracold atomic gas," Nature **397**, 594–598 (1999).
15. E. Paspalakis and P. L. Knight, "Electromagnetically induced transparency and controlled group velocity in a multilevel system," Phys. Rev. A **66**, 015802 (2002).
16. D. F. Phillips, A. Fleischhauer, A. Mair, and R. L. Walsworth, "Storage of light atom vapor," Phys. Rev. Lett. **86**, 783–786 (2001).
17. S. W. Su, Y. H. Chen, S. C. Gou, T. L. Horng, and I. A. Yu, "Dynamics of slow light and light storage in a Doppler-broadened electromagnetically-induced-transparency medium: a numerical approach," Phys. Rev. A **83**, 013827 (2011).
18. H. Wang, D. Goorskey, and M. Xiao, "Enhanced Kerr nonlinearity via atomic coherence in a three-level atomic system," Phys. Rev. Lett. **87**, 073601 (2001).
19. D. X. Khoa, L. V. Doai, D. H. Son, and N. H. Bang, "Enhancement of self-Kerr nonlinearity via electromagnetically induced transparency in a five-level cascade system: an analytical approach," J. Opt. Soc. Am. B **31**, 1330–1334 (2014).
20. L. V. Doai, D. X. Khoa, and N. H. Bang, "EIT enhanced self-Kerr nonlinearity in the three-level lambda system under Doppler broadening," Phys. Scripta **90**, 045502 (2015).
21. A. Joshi, A. Brown, H. Wang, and M. Xiao, "Controlling optical bistability in a three-level atomic system," Phys. Rev. A **67**, 041801 (R) (2003).
22. D. X. Khoa, L. V. Doai, L. N. M. Anh, L. C. Trung, P. V. Thuan, N. T. Dung, and N. H. Bang, "Optical bistability in a five-level cascade EIT medium: an analytical approach," J. Opt. Soc. Am. B **33**, 735–740 (2016).
23. M. A. Anton, F. Carreno, O. G. Calderon, S. Melle, and I. Gonzalo, "Optical switching by controlling the double-dark resonances in a N-tripod five-level atom," Opt. Commun. **281**, 6040–6048 (2008).
24. S. Ali, A. Ray, and A. Chakrabarti, "Double dark resonance in inverted Y system and its application in attenuating the optical switching action," Eur. Phys. J. D **70**, 27 (2016).
25. T. Chaneliere, D. N. Matsukevich, S. D. Jenkins, S.-Y. Lan, T. A. B. Kennedy, and A. Kuzmich, "Storage and retrieval of single photons transmitted between remote quantum memories," Nature **438**, 833–836 (2005).
26. F. Vewinger, J. Appel, E. Figuera, and A. Lvovsky, "Adiabatic frequency conversion of optical information in atomic vapor," Opt. Lett. **32**, 2771–2773 (2007).
27. S. R. de Echaniz, A. D. Greentree, A. V. Durrant, D. M. Segal, J. P. Marangos, and J. A. Vaccaro, "Observations of a doubly driven V system probed to a fourth level in laser-cooled rubidium," Phys. Rev. A **64**, 013812 (2001).
28. D. McGloin, D. J. Fullton, and M. H. Dunn, "Electromagnetically induced transparency in *N*-level cascade schemes," Opt. Commun. **190**, 221–229 (2001).
29. B. P. Hou, S. J. Wang, W. L. Yu, and W. L. Sun, "Double electromagnetically induced two-photon transparency in a five-level atomic system," Phys. Lett. A **352**, 462–466 (2006).
30. M. D. Lukin and A. Imamoglu, "Nonlinear optics and quantum entanglement of ultraslow single photons," Phys. Rev. Lett. **84**, 1419–1422 (2000).
31. Y. Li, C. Hang, L. Ma, and G. Huang, "Controllable entanglement of lights in a five-level system," Phys. Lett. A **354**, 1–7 (2006).
32. Y. Wu, J. Saldana, and Y. Zhu, "Large enhancement of four-wave mixing via EIT induced suppression of nonlinear photon absorptions," Phys. Rev. A **67**, 013811 (2003).
33. H. Yu, K. S. Kim, J. D. Kim, H. K. Lee, and J. B. Kim, "Observation of Doppler-free electromagnetically induced transparency in atoms selected optically with specific velocity," Phys. Rev. A **84**, 052511 (2011).
34. W. Xu and B. DeMarco, "Velocity-selective electromagnetically-induced-transparency measurements of potassium Rydberg states," Phys. Rev. A **93**, 011801 (2016).
35. R. Kumar, V. Gokhroo, and S. N. Chormaic, "Multi-level cascaded electromagnetically induced transparency in cold atoms using an optical nanofibre interface," New J. Phys. **17**, 123012 (2015).
36. A. Jagannathan, N. Arunkumar, J. A. Joseph, and J. E. Thomas, "Optical control of magnetic feshbach resonances by closed-channel electromagnetically induced transparency," Phys. Rev. Lett. **116**, 075301 (2016).
37. J. Wang, L. B. Kong, X. H. Tu, K. J. Jiang, K. Li, H. W. Xiong, Y. Zhu, and M. S. Zhan, "Electromagnetically induced transparency in multi-level cascade scheme of cold rubidium atoms," Phys. Lett. A **328**, 437–443 (2004).
38. L. V. Doai, P. V. Trong, D. X. Khoa, and N. H. Bang, "Electromagnetically induced transparency in five-level cascade scheme of ^{85}Rb atoms: an analytical approach," Optik **125**, 3666–3669 (2014).

39. D. X. Khoa, P. V. Trong, L. V. Doai, and N. H. Bang, "Electromagnetically induced transparency in a five-level cascade system under Doppler broadening: an analytical approach," Phys. Scripta **91**, 035401 (2016).
40. M. D. Eisaman, A. Andre, F. Massou, M. Fleischhauer, A. S. Zibrov, and M. D. Lukin, "Electromagnetically induced transparency with tunable single-photon pulses," Nature **438**, 837–841 (2005).
41. K. Cox, V. I. Yudin, A. V. Taichenachev, I. Novikova, and E. E. Mikhailov, "Measurements of the magnetic field vector using multiple electromagnetically induced transparency resonances in Rb vapor," Phys. Rev. A **83**, 015801 (2011).
42. K. G. Libbrecht and M. W. Libbrecht, "Interferometric measurement of the resonant absorption and refractive index in rubidium gas," Am. J. Phys. **74**, 1055–1060 (2006).
43. J. A. Souza, L. Cabral, R. R. Oliveira, and C. J. Villas-Boas, "Electromagnetically-induced-transparency-related phenomena and their mechanical analogs," Phys. Rev. A **92**, 023818 (2016).
44. Daniel Adam Steck, Rb85 D line data, http://steck.us/alkalidata.
45. M. Fleischhauer, A. Imamoglu, and J. P. Marangos, "Electromagnetically induced transparency: optics in coherent media," Rev. Mod. Phys. **77**, 633–673 (2005).

137.132.123.69 {ts '2017-05-24 23:35:13'}